SPECIAL TOPIC — International Conference on Nanoscience & Technology, China 2013

Synthesis of boron, nitrogen co-doped porous carbon from asphaltene for high-performance supercapacitors*

Zhou Ying(周 颖)†, Wang Dao-Long(王道龙), Wang Chun-Lei(王春雷), Jin Xin-Xin(金新新), and Qiu Jie-Shan(邱介山)

Carbon Research Laboratory, Liaoning Key Laboratory for Energy Materials and Chemical Engineering, State Key Laboratory of Fine Chemicals, Dalian University of Technology, Dalian 116024, *China*

(Received 4 September 2013; revised manuscript received 28 January 2014; published online 10 June 2014)

Oxidized asphaltene (OA), a thermosetting material with plenty of functional groups, is synthesized from asphaltene (A) using HNO_3/H_2SO_4 as the oxidizing agent. Boron, nitrogen co-doped porous carbon (BNC–OA) is prepared by carbonization of the mixture of boric acid and OA at 1173 K in an argon atmosphere. X-ray photoelectron spectroscopy (XPS) characterization reveals that the BNC–OA has a nitrogen content of 3.26 at.% and a boron content of 1.31 at.%, while its oxidation-free counterpart (BNC–SA) has a nitrogen content of 1.61 at.% and a boron content of 3.02 at.%. The specific surface area and total pore volume of BNC–OA are 1103 $m^2 \cdot g^{-1}$ and 0.921 $cm^3 \cdot g^{-1}$, respectively. At a current density of 0.1 $A \cdot g^{-1}$, the specific capacitance of BNC–OA is 335 $F \cdot g^{-1}$ and the capacitance retention can still reach 83% at 1 $A \cdot g^{-1}$. The analysis shows that the superior electrochemical performance of the BNC–OA is attributed to the pseudocapacitance behavior of surface heteroatom functional groups and an abundant pore-structure. Boron, nitrogen co-doped porous carbon is a promising electrode material for supercapacitors.

Keywords: boron–nitrogen co-doped porous carbon, asphaltene, preparation, supercapacitors

PACS: 61.43.Gt, 81.05.U–, 82.47.Uv, 81.02.–n **DOI:** 10.1088/1674-1056/23/8/086101

1. Introduction

Supercapacitors have received much attention because of their high power density, fast recharge capability, and long life cycle, which have been widely used in telecommunication devices, such as cell phones and pagers, stand-by power systems and electric/hybrid vehicles.[1,2] Among the various electrode candidates for supercapacitors, porous carbon is the most promising material owing to its high surface area, excellent physico–chemical stability, easy availability, and cost-effectiveness.[3,4] For carbon-based materials as supercapacitors electrodes, the capacitance mainly comes from the pure electrostatic charge accumulated at the electrode/electrolyte interface, which is closely related to their pore-structure and surface chemical properties.[5] In order to enhance the capacitance to meet the application in tomorrow's high-energy devices, doping heteroatoms like oxygen,[6] nitrogen,[7] boron,[8] phosphorus,[9] and sulfur[10] into carbon materials is an effective way. Among them, nitrogen and boron are more promising foreign atoms for enhancing capacity.[11,12] These atoms can modify the electron donor–acceptor properties of the carbon, which in turn provides pseudocapacitive faradaic reactions.[13]

Heavy carbon resources (HCRs) like asphaltene (A), exhibiting an excellent graphitizable property, high carbonization yield, and little ash content, are commonly used in carbon industries.[14] Here, we report a simple approach to preparing porous carbon enriched with nitrogen and boron through carbonization of the mixture of boric acid and oxidized asphaltene (OA). The structure, surface chemical properties, and electrochemical performance of as-made carbons are discussed.

2. Experiment

2.1. Preparation of samples

BNC–OA was synthesized by the carbonization of a mixture containing boron acid and OA under an argon atmosphere using boron acid as the dopant and pore-forming agent. The OA was prepared according to Ref. [15]. Typically, OA and boric acid (AR grade) were dissolved in distilled water by stirring until the excess water was removed. The resulting brown powders were placed into a tube furnace and carbonized in Ar flow at a heating rate of 5 $K \cdot min^{-1}$ to 1173 K for 1 h. Then the products were boiled in 1-M NaOH to dissolve the borate by-products, filtrated and dried at 383 K for 24 h. For comparison, BNC–SA was prepared from stabilized asphaltene (SA) which was prepared by heat treatment of A at 400 °C for 2 h in air, following the same procedure.

2.2. Physico-chemical characterization of samples

Crystallite structures of samples were determined by X-ray diffraction (XRD, D/MAX-2400) using Cu K_α radiation from 5° to 80° angles. Morphologies and microstructures of

*Project supported by the National Natural Science Foundation of China (Grant No. 21276045).

†Corresponding author. E-mail: zhouying.dlut@dlut.edu.cn

© 2014 Chinese Physical Society and IOP Publishing Ltd

samples were examined by a field emission scanning electron microscope (FE-SEM, FEI NOVA NanoSEM 450, operated at 3 kV) and a transmission electron microscope (TEM, FEI TF30, operated at 300 kV). The element distribution investigations were examined by an Oxford X-MAX energy dispersive X-ray spectroscope (EDS, FEI QUANTA450, operated at 20 kV). The pore-structure was investigated by physical adsorption of N_2 at 77 K (Micromeritics ASAP2020). Samples were degassed at 523 K for 5 h prior to the measurement. The specific surface area (SSA) of samples was calculated using the Brunauer–Emmett–Teller (BET) method within a relative pressure range of 0.05∼0.20. The pore size distribution (PSD) of samples was derived from the density functional theory (DFT) model. The total pore volume (V_{tot}) was estimated from single point adsorption at a relative pressure P/P_0 of 0.995. The surface chemical compositions of samples were analyzed by X-ray photoelectron spectroscopy (XPS, VG ESCALAB 250) with an Al K_α monochromatic source (15 kV, 10 mA).

2.3. Electrochemical measurements

Electrodes were made by using acetylene black (10 wt%) as an electrical conductor, polytetrafluoroethylene (PTFE) (5 wt%) as a binder, and nickel foam as current collectors. The diameter of the electrode was 8 mm and the mass was between 4.0 mg and 5.5 mg. Electrochemical measurements were performed in 6-M KOH at room temperature in a three-electrode system using the as-made electrode as the working electrode, the platinum plate as a counter electrode and Hg/HgO as a reference electrode. Cyclic voltammetry (CV) and galvanostatic charge–discharge measurements were performed with a potential window from −1 V to 0 V by the CHI660C electrochemical work station (Shanghai Chenhua) and the Land CT2001A battery test system (LAND, Wuhan), respectively. The specific gravimetric capacitance was calculated according to the charge/discharge tests based on the following equation:

$$C = (I \cdot \Delta t)/(m \cdot \Delta V),$$

where C is the specific gravimetric capacitance (F/g), I is the discharge current (A), Δt is the discharge time (s), ΔV is the potential difference (V), and m is the mass (g) of the active electrode material. Electrochemical impedance spectroscopy (EIS) measurement was carried out at an open circuit potential in the frequency range from 0.01 Hz to 100 kHz.

3. Results and discussion

3.1. Physico-chemical characteristics of samples

The XRD patterns are shown in Fig. 1. In the patterns, there are two diffraction peaks around 2θ of 26° and 43°, corresponding to the diffraction of (002) and (100) planes, respectively. The two peaks of BNC–OA are broader and fainter than those of BNC–SA, implying the low crystallinity. The possible reason for this is that the synthesis of BNC–SA from SA is a liquid-phase carbonization, which is beneficial to the formation of graphitizable carbon. However, OA is a thermosetting powder and experiences a solid-phase carbonization process from OA to BNC–OA, which is adverse to the graphite crystallite orientation and thus results in its low crystallinity.

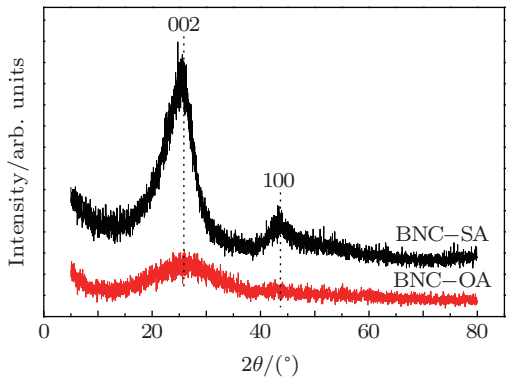


Fig. 1. (color online) X-ray diffraction patterns for samples.

The SEM and TEM images of the samples are shown in Fig. 2. It is easy to find the differences in particle size and morphology between the two samples (Figs. 2(a) and 2(b)). The particle size of BNC–SA is larger than BNC–OA. The surface of BNC–SA is composed of many sharp edges and an abundant micro-scale pore-structure, whereas the surface of BNC–OA possesses a smooth blocky structure, which is surrounded by continuous sponge-like microripple structures (see the inset in Fig. 2(b)). As seen in Fig. 2(c), BNC–SA consists of carbon layers which are loaded with some spherical morphologies and the inset reveals that the arrangement of microcrystallites is rather ordered in a certain orientation. However, figure 2(d) shows BNC–OA consists of small particles which connect to each other and form an aggregate with an irregular shape. The inset shows the BNC–OA has an abundant nano-sized pore-structure and the graphitic crystallites are arranged in a disorderly way, which presents a turbostratic structure. Thus, the results of TEM are in good agreement with the analyses of XRD.

The N_2 adsorption/desorption isotherms and the corresponding DFT PSDs curves of the samples are shown in Fig. 3. Figure 3(a) indicates that the pore-structure of BNC–SA is underdeveloped. However, BNC–OA exhibits a porous structure. As seen from the isotherm of BNC–OA, the sharp increase of N_2 adsorbed at the low relative pressure close to 0.01 suggests the formation of micropores, the small hysteresis loop and the continuous accretion of nitrogen adsorbed at the relative pressure from 0.45 to 1.0 indicate the formation of a mesoporous structure and the occurrence of macroporosity. The PSD curves in Fig. 3(b) strongly corroborate the above-mentioned views.

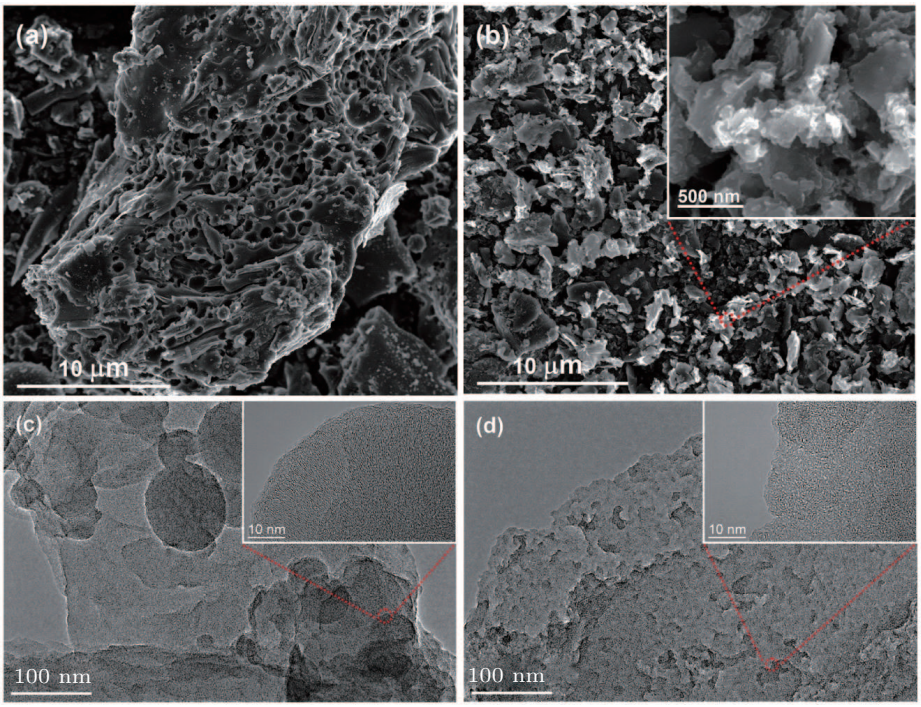


Fig. 2. (color online) SEM images of (a) BNC–SA and (b) BNC–OA with the expanded SEM image in the inset; TEM images of (c) BNC–SA and (d) BNC–OA each with their corresponding HRTEM image in the inset.

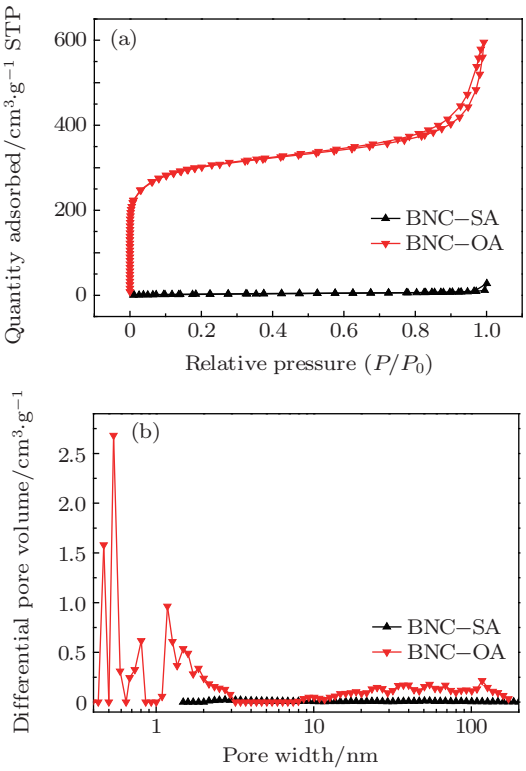


Fig. 3. (color online) (a) N_2 adsorption/desorption isotherms and (b) DFT pore size distributions of samples.

The pore-structure parameters are listed in Table 1. The SAA of BNC–OA is as large as 1103 $m^2 \cdot g^{-1}$, which is much larger than that of BNC–SA. It can be attributed to the characteristics of the OA precursor. Firstly, the OA is dispersed in water easily as nano-scale particles, which can interact with H_3BO_3 in an aqueous solution due to a great number of oxygen-containing groups in the surface of the OA.[16] Secondly, the OA is a thermosetting solid to avoid softening during the carbonization and the softening will hinder the formation of the pore-structure.

Table 1. Pore-structure parameters and heteroatom content values of samples.

Samples	S_{BET} /$m^2 \cdot g^{-1}$	V_{tot} /$cm^3 \cdot g^{-1}$	XPS analysis	
			N/at.%	B/at.%
BNC–SA	13	0.043	1.61	3.02
BNC–OA	1103	0.921	3.26	1.31

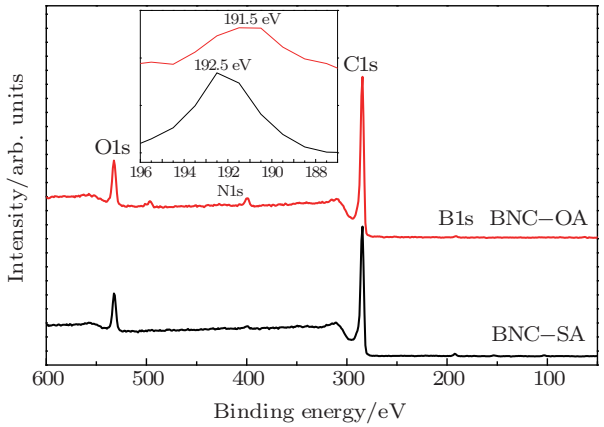


Fig. 4. (color online) X-ray photoelectron spectroscopy patterns of samples.

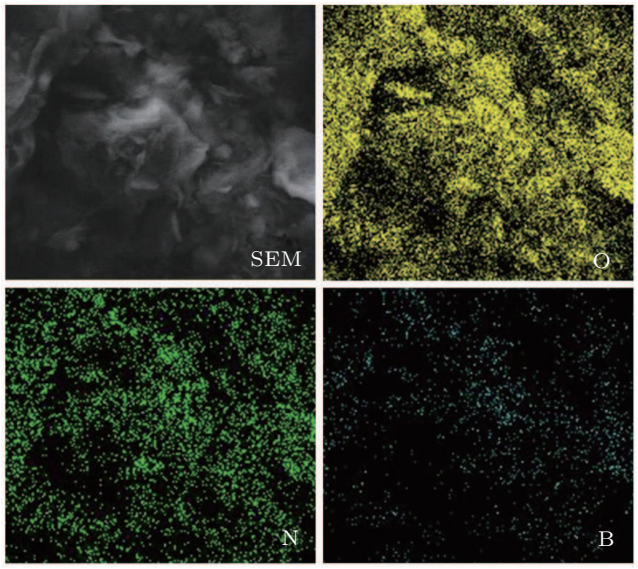


Fig. 5. (color online) The SEM mappings of BNC–OA.

The heteroatom content values of samples are studied by XPS (Fig. 4). Results show that BNC–OA and BNC–SA are doped with both boron and nitrogen with the binding energy peaks appearing at about 192 eV and 399 eV, respectively. But their content values and binding energies are different. BNC–OA has the nitrogen content of 3.26 at.%, which is larger than BNC–SA, which is attributed to the nitration produced concurrently in the oxidation process. The chemical states of the B, N co-doped and separately doped boron samples are different and their binding energies are 191.5 eV and 192.5 eV, respectively.[17] The nitryl in the OA can interact with H_3BO_3, forming the N–B bond at the periphery of the graphite sheet and then finally achieving the B, N co-doped material. But BNC–SA just has the B and N doped solely. What is more, the EDS mapping in Fig. 5 indicates that oxygen, nitrogen, and boron atoms distributing in the surrounding microripple structures are more dense than in a blocky structure, which is coincident with the scenario of the heteroatom functional groups distributed at the periphery of graphite sheets.

3.2. Electrochemical characterization of samples

The cycle voltammetry (CV) technique is employed to monitor the electrochemical behaviors of the samples. From Fig. 6(a), wide humps can be clearly observed on the CV curves of BNC–OA, which exhibits the presence of pseudocapacitance. Because the nitrogen atoms at the periphery of the graphene layers provide electron pairs, which may introduce electron donor properties into the layer and the deficiency of electrons for boron may introduce electron hole properties. However, the CV curve of BNC–SA exhibits a small distorted rectangular curve due to its underdeveloped pore-structure.

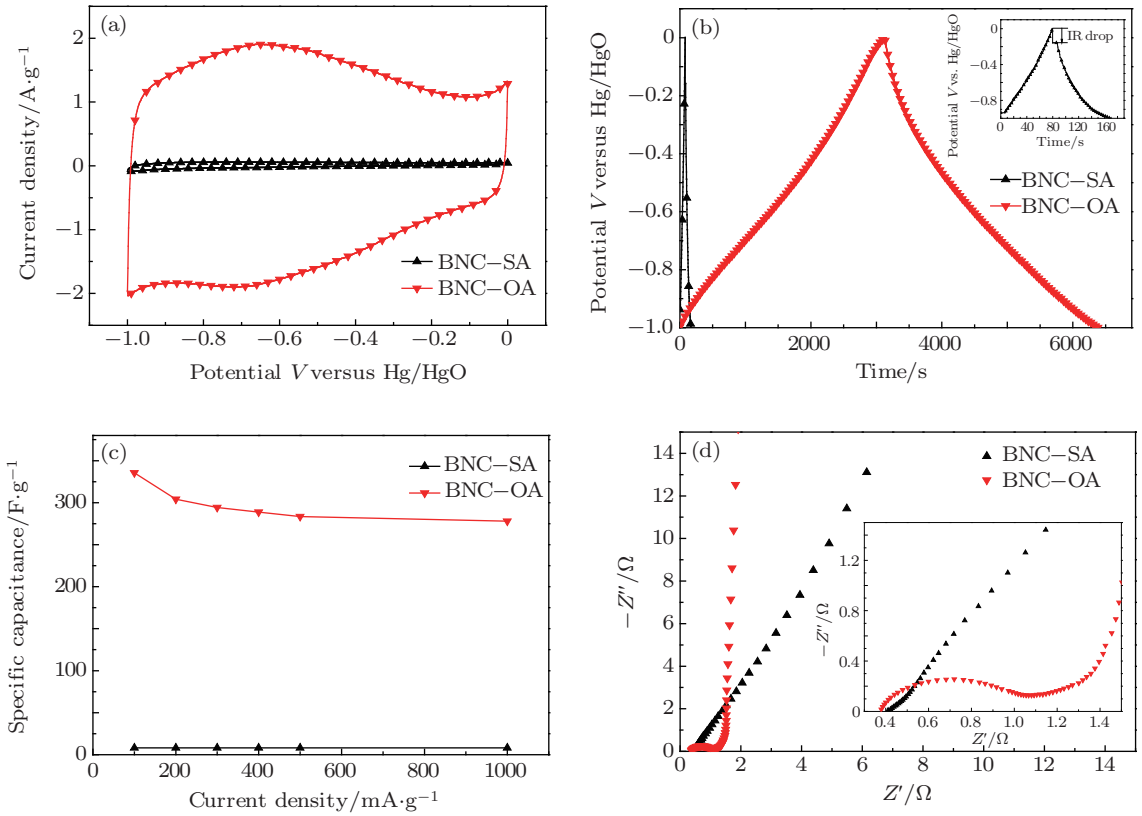


Fig. 6. (color online) (a) CV curves at a scan rate of 5 mV·s^{-1}, (b) galvanostatic charge–discharge curves at a current density of 0.1 A·g^{-1}, (c) relationships between specific capacitance and current density, and (d) Nyquist plots in the frequency range of 100 kHz–10 MHz (the inset shows the expanded high-frequency region of the plot) of BNC–SA and BNC–OA.

Figure 6(b) shows the typical charge/discharge curves of samples at a current density of 0.1 $A{\cdot}g^{-1}$. BNC–OA shows a longer charge/discharge time, indicating its higher specific capacitance than that of BNC–SA. The specific capacitance of BNC–OA is as large as 335 $F{\cdot}g^{-1}$ at a current of 0.1 $A{\cdot}g^{-1}$ due to its high SSA and pseudocapacitive behaviors of the nitrogen and boron functional groups. Figure 6(c) shows the relationship between specific capacitance and current density. Specific capacitance decreases slightly with the increase of current density. When the current density is increased from 0.1 $A{\cdot}g^{-1}$ to 1 $A{\cdot}g^{-1}$, the capacitance still remains at 83% for BNC–OA. By comparison with capacitance, the BNC–OA electrode shows a more outstanding electrochemical performance than BNC–SA. Figure 6(d) shows the Nyquist plot and the expanded high-frequency region of the plot of samples. The BNC–OA electrode presents a nearly vertical straight line at low frequency and a small semicircle in a high frequency range, evincing a good capacitive behavior. In general, heteroatom-enriched porous carbons with a high surface area prepared from OA are desirable electrode materials for supercapacitors.

4. Conclusions

BNC–OA with a high surface area is prepared from the OA using boric acid as the dopant and pore-forming agent. The hydrophilic groups of the OA introduced by the oxidation process make the OA disperse and interact with the H_3BO_3 aqueous solution easily. The BNC–OA with a nitrogen content of 3.26 at.%, a boron content of 1.31 at.% and the SSA as high as 1103 $m^2{\cdot}g^{-1}$ shows the highest capacitance of 335 $F{\cdot}g^{-1}$ in the 6-M KOH electrolyte at a current density of 0.1 $A{\cdot}g^{-1}$. Even when the current density is raised up to 1 $A{\cdot}g^{-1}$, the capacitance is still as high as 278 $F{\cdot}g^{-1}$. In conclusion, it is the special characteristics of OA that make the BNC–OA a competitive electrode material for supercapacitors.

References

[1] Miller J R and Simon P 2008 *Science* **321** 651
[2] Burke A 2000 *J. Power Sources* **91** 37
[3] Frackowiak E and Béguin F 2001 *Carbon* **39** 937
[4] Pandolfo A G and Hollenkamp A F 2006 *J. Power Sources* **157** 11
[5] Kötz R and Carlen M 2000 *Electrochim. Acta* **45** 2483
[6] Nian Y R and Teng H S 2002 *J. Electrochem. Soc.* **149** A1008
[7] Jurewicz K, Babel K, Źiólkowski A and Wachowska H 2003 *Electrochim. Acta* **48** 1491
[8] Wang D W, Li F, Chen Z G, Lu G Q and Cheng H M 2008 *Chem. Mater.* **20** 7195
[9] Hulicova-Jurcakova D, Puziy A M, Poddubnaya O I, Suárez-García F, Tascon J M D and Lu G Q 2009 *J. Am. Chem. Soc.* **131** 5026
[10] Seredych M and Bandosz T J 2013 *J. Mater. Chem. A* **1** 11717
[11] Guo H L and Gao Q M 2009 *J. Power Sources* **186** 551
[12] Konno H, Ito T, Ushiro M, Fushimi K and Azumi K 2010 *J. Power Sources* **195** 1739
[13] Kwon T, Nishihara H, Itoi H, Yang Q H and Kyotani T 2009 *Langmuir* **25** 11961
[14] Zhang W F, Huang Z H, Cao G P, Kang F Y and Yang Y S 2012 *J. Phys. Chem. Solids* **73** 1428
[15] Tateishi D, Esumi K and Honda H 1991 *Carbon* **29** 1296
[16] Ito H, Kono Y, Machida A, Mitsumoto Y, Omori K, Nakamura N, Kondo Y and Ishihara K 2003 *Inorg. Chim. Acta* **344** 28
[17] Ozaki J I, Kimura N, Anahara T and Oya A 2007 *Carbon* **45** 1847